

Journal of Materials Chemistry A

Accepted Manuscript



This is an *Accepted Manuscript*, which has been through the Royal Society of Chemistry peer review process and has been accepted for publication.

Accepted Manuscripts are published online shortly after acceptance, before technical editing, formatting and proof reading. Using this free service, authors can make their results available to the community, in citable form, before we publish the edited article. We will replace this *Accepted Manuscript* with the edited and formatted *Advance Article* as soon as it is available.

You can find more information about *Accepted Manuscripts* in the [Information for Authors](#).

Please note that technical editing may introduce minor changes to the text and/or graphics, which may alter content. The journal's standard [Terms & Conditions](#) and the [Ethical guidelines](#) still apply. In no event shall the Royal Society of Chemistry be held responsible for any errors or omissions in this *Accepted Manuscript* or any consequences arising from the use of any information it contains.



Journal Name

ARTICLE

CdSe on a Mesoporous Transparent Conducting Oxide Scaffold as a Photocathode

Received 00th January 20xx,
Accepted 00th January 20xx

Michael R. Norris^a and Brandi M. Cossairt^a

DOI: 10.1039/x0xx00000x

We report here a photocathode based on a high surface area conductive metal oxide scaffold sensitized by CdSe quantum dots attached via organic linkers. Photoreduction of methyl viologen demonstrates efficient photoreactions occurring at electrode surfaces and verifies that the high surface area scaffold is promising for use as a photocathode material.

www.rsc.org/

Introduction

Rising energy demands and the need to decrease CO₂ emissions require the utilization of alternative energy resources. For solar energy to become viable on a global scale, energy storage solutions are necessitated by the intermittent and diffuse nature of sunlight. An avenue toward energy storage would be to use sunlight to create chemical bonds through the reduction of protons or CO₂ to energy dense fuels, mimicking processes occurring in natural photosynthesis.¹ This artificial photosynthetic construct would thus require a photoanode (water oxidation) and a photocathode (H⁺ or CO₂ reduction) as shown in Figure 1. As attractive as this concept sounds, design of a practical device on a large scale remains a formidable challenge as it is important to carefully control both the band gaps and relative band edge positions of the photoanode and photocathode in order to both meet the thermodynamic considerations for water splitting, and absorb complementary photons to increase device efficiency.²

Due to the ability to control the optical and electronic properties of semiconductor quantum dots (QDs) through size selective synthesis, QDs are ideal materials to be used for light absorption in photocathode and photoanode applications.³ QDs, particularly CdSe and CdS, have been used effectively in dye-sensitized solar cells where the QDs are attached to TiO₂ and light absorption initiates electron injection into the TiO₂ CB to create charge separation. These systems naturally have been applied as photoanodes for a variety of device architectures for generating current from light.⁴ For fuel production, these photovoltaic (PV) materials have been coupled to photoelectrochemical cells (PEC) using combinations of QD materials and dye-sensitized solar cells to generate the necessary photovoltage for proton reduction.⁵

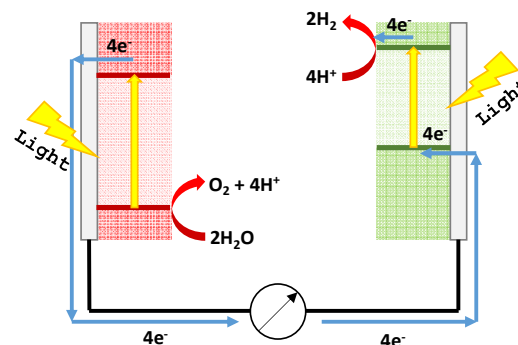


Figure 1. Illustration of a z-scheme device containing a photoanode for water oxidation and a photocathode for proton reduction. The electrodes may each consist of multiple components.

In addition to being utilized as sensitizers on n-type TiO₂ for PV and PEC applications, QDs have also been shown to drive H⁺ reduction catalysts.^{6,7} However, examples of photocathodes where these materials are used to sensitize wide band gap p-type semiconductors and drive H⁺ reduction heterogeneously remain rare. One difficulty in the design of photocathodes is the relative dearth of wide band gap p-type semiconductors to use analogously to TiO₂. NiO has been the most popular candidate but it is not as effective as TiO₂ given issues relating to poor sensitizer loading, fast (ps) back electron transfer from the dye to injected holes, and lower carrier mobilities.⁸ Further, syntheses of high-surface area electrodes of NiO with nanoscale structural control have proven difficult. Other p-type materials, such as InP nanowire arrays, have been combined with H⁺ reduction catalysts for photoelectrochemical H₂ production.⁹ Unfortunately, these are not quantum confined and the band gap is not tuneable.

^a University of Washington, Department of Chemistry, Box 351700, Bagley Hall, Seattle, WA 98195-1700, USA

† E-mail: cossairt@chem.washington.edu

Electronic Supplementary Information (ESI) available: figures and pictures of experimental set-up. See DOI: 10.1039/x0xx00000x

In order to address the issues of photocathode construction, we sought to design an easily tailored system with QDs anchored to a transparent and high surface-area electrode. The material of choice was a mesoporous film of tin-doped indium oxide (*nanITO*). Electrodes of this material are easily made through spin coating a suspension of commercially available nanoparticles followed by annealing, and the electrodes have been shown to be transparent and conductive.¹⁰ The hypothesis for use of this material was that CdSe QDs, shown to be effective at light-driven reduction reactions (specifically the hydrogen evolution reaction) in solution,⁶ would continue to function as such when on a surface.

Results and Discussion

CdSe QDs were synthesized via a heat-up method wherein a mixture of cadmium myristate and selenium dioxide are suspended in octadecene and heated to 220 °C.¹¹ Addition of oleic acid to cease growth, followed by precipitation with acetone gave zinc blende CdSe QDs with a 3.4 nm diameter as determined by the position of the lowest-energy excitonic transition (LEET) as has previously been reported.¹²

In order to sensitize the electrodes with the CdSe QDs, a method of dip-coating ligand exchange was used. First, a 30 × 10 mm electrode with a 10 × 10 mm active area was immersed in a 0.1 M methanolic solution of 3-mercaptopropionic acid (MPA) for 10 min. It is known that carboxylate¹³ and phosphonate¹⁰ functionalities readily bind to *nanITO* electrodes and it was surmised that the MPA would bind through the carboxylic acid. The electrode was then rinsed with methanol, dried, and dipped into a 5.0 × 10⁻⁷ M solution of CdSe QDs in pentane for 10 min. After immersion, the electrode was rinsed with pentane and visibly had turned a light orange. This two-step dipping procedure was then repeated two additional times. Importantly, soaking the slides in pentane (or aqueous PBS buffer as used in the photochemical studies) does not result in loss of CdSe QDs from the surface after binding to the organic linkers. In addition, the CdSe QDs are not simply physisorbed to the surface as soaking a *nanITO* electrode in CdSe QDs for 2 h without first soaking the electrode in an organic ligand led to significantly less absorbance (Figure S2).

Figure 2 shows the UV/vis spectra of the solution of pentane containing CdSe used to load the electrodes as well as the resulting electrode after 3 loading cycles. The UV/vis spectrum shows CdSe attached to the slide and the feature from the LEET remains centered at 563 nm with slight broadening. The broadening may be due in part to the scattering of the CdSe on the solid support or the presence of random orientations on the surface, although it is likely that the ligand exchange perturbs the surface states leading to a difference in absorption. A variety of additional bi-functional organic linkers including 1,2-ethylenediphosphonic acid, 4-aminobenzylphosphonic acid, and terephthalic acid were used to tether CdSe to *nanITO* electrodes using the described procedure (see Figure S3). Each of these binds the *nanITO*

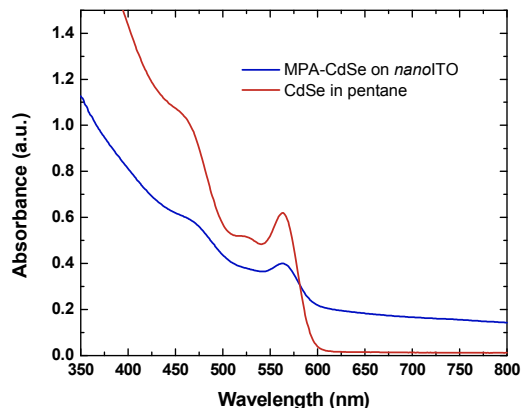


Figure 2. UV/vis absorption of a solution of CdSe in pentane (red) and CdSe attached to a *nanITO* electrode (blue). The electrode was held in the path of the beam without any solvent.

through either phosphonic acid or carboxylic acid moieties and the CdSe then binds through either a phosphonic acid (1,2-ethylenediphosphonic acid), primary amine (4-aminobenzylphosphonic acid), or carboxylic acid (terephthalic acid) head group. Each ligand binding the CdSe to the *nanITO* surface results in slight variation of the UV/vis absorption with a hypsochromic shift and increased broadening observed in the order $-S < -COOH < -NH_2 < -PO_3H_2$. For the majority of the studies described in this paper, MPA ligands were used as they displayed the smallest perturbation from the solution absorption spectrum. In addition, MPA was conveniently used as a sacrificial donor in the photochemical experiments.

The electrodes were also characterized by electron microscopy. Figure 3 shows a picture of the *nanITO* film before and after annealing in forming gas and after loading with CdSe (A), and SEM images of both the bare *nanITO* film (B) and *nanITO* film loaded with CdSe QDs (C). The images illustrate the adherence of the CdSe QDs to the film with retention of transparency. The SEM images confirm the mesoporous nature of the annealed *nanITO* films and that attachment of the CdSe QDs to the surface has little effect on the film morphology.

A combination of UV/vis spectroscopy and electrochemical measurements were used to determine the active surface area of the modified *nanITO* electrodes. UV/vis spectra of CdSe bound via the MPA linker to both planar fluoride-doped tin oxide (FTO) and *nanITO* (geometric active area of 10 mm × 10 mm) – both were loaded with 3 dipping cycles–

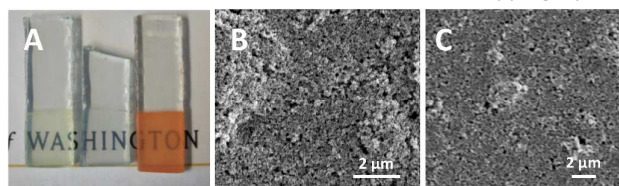


Figure 3. A) Photograph of *nanITO* electrodes (from left to right) annealed in air, after a second anneal under forming gas, and after sensitization with CdSe. B) SEM image of a *nanITO* electrode as synthesized. C) SEM image of a *nanITO* electrode with CdSe attached.

were compared (Figure S4). The maximum absorbance of the LEET of the *nano*ITO slide is ca. 3× that of the LEET absorbance of the planar FTO slide. For electrochemical comparison, a viologen derivatized with a propionic acid group was anchored to both the planar FTO and *nano*ITO electrodes using the same dipping technique in a solution of 0.1 M viologen in methanol. This allows the viologen to bind to the surface of the electrodes. The viologen-derivatized electrodes were then used in a three electrode cell as the working electrode, with a platinum counter, and Ag/AgNO₃ reference electrode in a 0.1 M acetonitrile solution of tetrabutylammonium hexafluorophosphate. Reductive scans show two reversible couples corresponding to the reduction of the viologen first to the radical cation followed by the di-radical (Figure S5). The amount of current passed was determined by the area under the cathodic peaks. For the *nano*ITO, the current passed was ca. 3.7× that of the planar FTO slide. Finally, chronocoulometry was used to generate Anson plots of the oxidation of ferrocene by the bare *nano*ITO electrodes to determine active surface area. For these experiments, *nano*ITO electrodes were used as the working electrode with a 10 mM ferrocene standard. A potential step experiment was used to instantaneously step to a potential sufficient to oxidize all the ferrocene. The total charge (Q) that passes during the time following a potential step is measured as a function of time (Figure S6). For a diffusionally controlled system, the charge observed following the potential step can be described by the integrated Cottrell equation, known as the Anson equation:

$$Q = 2nFACD^{1/2} \pi^{-1/2} t^{1/2}$$

A plot of Q vs. $t^{1/2}$ (Figure S7) thus gives a straight line with the slope being equal to:

$$2nFACD^{1/2} \pi^{-1/2}$$

where n is the number of moles of electrons in the redox reaction, F is Faraday's constant, C is the concentration of substrate (ferrocene), and D is the diffusion coefficient ($2.3 \times 10^{-5} \text{ cm}^2/\text{s}$ for ferrocene under the experimental conditions). This analysis gave a surface area of 2.2× that of the geometric surface area, although this method can underestimate the active surface area of mesoporous electrodes when a fast electron transfer mediator is used.¹⁴

In order to assess the performance of the CdSe QDs for driving reduction reactions, photoreduction experiments were conducted with a suspension of CdSe QDs, MPA as a sacrificial electron donor, and methyl viologen (MV^{2+}) as an electron acceptor. Methyl viologen was chosen as it has a first reduction potential at -0.45 V vs NHE (Figure S8), a potential that is sufficiently reducing to drive proton reduction to H₂. In addition, the radical cation generated ($\text{MV}^{+\bullet}$) is an intense purple color that can be monitored spectrophotometrically. Experiments were designed such that a QD solution could be irradiated with LEDs to generate an exciton. An electron would then transfer from the excited QD to the MV^{2+} and the

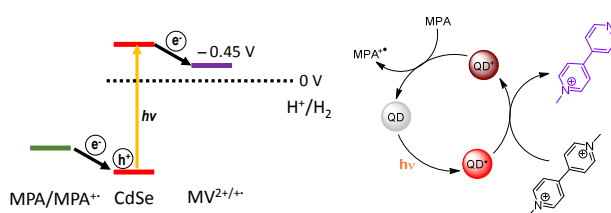


Figure 4. Cartoon of the relative energy levels of the CdSe conduction and valence bands, the oxidation potential of the sacrificial donor (MPA), the $\text{MV}^{2+/\bullet}$ couple, and the proton reduction couple at pH = 0 (left), and diagram of the photoexcitation, reduction, regeneration cycle (right).

hole would be trapped by the MPA, thus regenerating the CdSe ground state (Figure 4). Alternatively it is possible that the donor (MPA) quenches the excited QD followed by a rapid electron transfer from the QD(e⁻) to the MV^{2+} . Although MV^{2+} reduction is a bimolecular process, MV^{2+} has been demonstrated to pre-associate with the QD surface, and CdS- MV^{2+} systems have been shown to undergo photoinduced electron transfers with rate constants¹⁴ of $1.2 \times 10^{10} \text{ s}^{-1}$, while hole trapping rates can range on the order of 1 ps to 50 ns.^{15,16} The initial experiments were done as a benchmark for the surface reactions with the sensitized *nano*ITO electrodes.

For each photoreduction experiment, a solution of CdSe QDs ($1.6 \times 10^{-8} \text{ mol}$), 5 mM $[\text{MV}](\text{I})_2$, and 50 mM MPA in pH 7.4 phosphate buffered aqueous solution were illuminated with a strip of LEDs (Figure S9). The surface of the CdSe dots in this experiment is likely a mixture of the MPA ligands and native oleate ligands. Initial exchange of oleate ligands for all MPA ligands before the experiment led to solutions of CdSe QDs that were not colloiddally stable and quickly aggregated under the reaction conditions. Improved colloiddal stability was realized by suspension of CdSe QDs with oleate ligands in the photoreduction solution via sonication for 5 minutes (presumably resulting in partial ligand exchange). The reaction was monitored by UV/vis at various time points to observe the appearance of the $\text{MV}^{+\bullet}$. The radical cation has a known extinction coefficient of $13700 \text{ M}^{-1}\text{cm}^{-1}$ at 603 nm¹⁷ in water that could be used to calculate the amount of $\text{MV}^{+\bullet}$ produced at any given time. The amount of $\text{MV}^{+\bullet}$ produced was monitored over 20 minutes and the experiment was run 3 times. The number of moles of $\text{MV}^{+\bullet}$ produced was divided by the number of moles of CdSe in the reaction to give the turnovers per CdSe QD where a turnover is a photon absorption followed by electron transfer to generate the $\text{MV}^{+\bullet}$. These results are plotted in Figure 5 (red squares) with error bars for the three trials, and show an increase in $\text{MV}^{+\bullet}$ with time consistent with the series of events depicted in Figure 4. After 2 minutes the rate of $\text{MV}^{+\bullet}$ production begins to slow and the plot begins to plateau. This behaviour likely has two main causes, the first being an imperfect seal on the vessel and a slow leak of atmosphere which will re-oxidize some of the $\text{MV}^{+\bullet}$, and the second due to the intense purple color of the solution which, at high $\text{MV}^{+\bullet}$ concentrations, competitively absorbs the LED light.

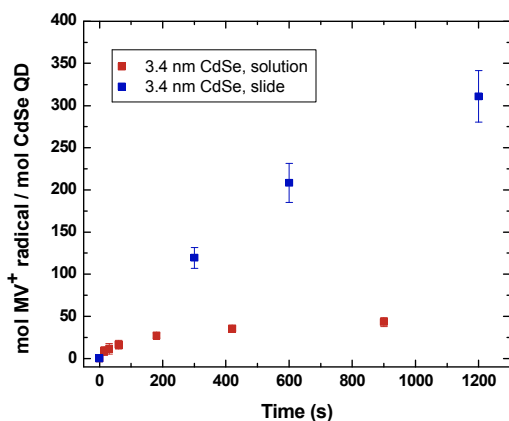


Figure 5. Plot of the generation of $MV^{\bullet+}$ over time using a white LED with both a suspension of CdSe (red) and a *nanoITO* slide with attached CdSe (blue) in pH = 7.4 aqueous phosphate buffer with 5 mM MV^{2+} and 50 mM MPA.

The photoreduction quenching experiments were repeated with the same composition of pH 7.4 aqueous solution containing MPA and $[MV](I)_2$ but instead of a suspension of CdSe QDs, a *nanoITO* slide that had been loaded with three cycles of dipping was added to the vessel. The same illumination experiment was conducted, again showing the generation of $MV^{\bullet+}$ with time. The experiments were repeated 3 times, utilizing fresh solutions of MPA and MV^{2+} and rinsing slides in between trials. Although the role of MPA as the sacrificial donor involves coupling of S-S bonds in an irreversible oxidation step to refill the holes on the QDs, appreciable loss of CdSe from the surface was not observed by UV/vis spectroscopy. It should also be noted that similar to the solution experiments, some fraction of native oleate ligands are likely still bound to the QDs at the beginning of the experiment. Data from these trials are also plotted in Figure 5 (blue squares) with error bars from 3 separate experiments. In order to calculate the moles of CdSe on the slide for comparison to the solution experiments, a geometric approximation was made. Given that the packing efficiency of circles in a 2-D space is 91%; the diameter of the dots (3.4 nm) and the geometric surface area of the electrode (1 cm^2) were used to calculate the number of CdSe QDs that could be placed in that area. This number was then multiplied by 4, given that the actual active area of the mesoporous *nanoITO* electrode was found to be 2 – 5 times that of the geometric surface area which gives 1.8×10^{-17} mol of QDs (9 orders of magnitude less than in the solution experiments). While this gave an estimate as to the number of CdSe QDs on the surface, it is important to note that it likely *overestimates* the number of QDs on the surface, given that the packing efficiency of the QDs in the mesoporous film is much less than 91%. Strikingly, the reduction of the MV^{2+} to $MV^{\bullet+}$ is not impeded at the surface and the number of molecules of $MV^{\bullet+}$ produced per QD is an order of magnitude larger than the QD suspension. Control experiments of non-functionalized *nanoITO* slides illuminated under the same conditions showed no production of $MV^{\bullet+}$ over 20 minutes. The difference of photochemical reduction

reactions at CdSe on a surface versus in solution in this instance is likely a function of the actual number of CdSe QDs available; with the solution experiments having 5 – 7 orders of magnitude more QDs. One possible reason for the poorer performance of the CdSe solutions is the statistical probability of a reduced $MV^{\bullet+}$ encountering an excited QD, which would be capable of re-oxidizing the $MV^{\bullet+}$ in a non-productive process. More importantly, these data are indicative of the ability to drive important reduction reactions photochemically at the surface of an electrode.

Finally, we wanted to replace the sacrificial donors used in the system with an electrochemical bias. Since in an overall water-splitting device electrons would be delivered via wire to a photocathode for fuel production, photoelectrochemical reduction of MV^{2+} would represent a proof of concept for use of this material as a photocathode. For these experiments, a *nanoITO* slide derivatized with CdSe QDs was used as a working electrode in a 3-electrode cell with the solution containing the same mixture of MV^{2+} and phosphate buffer, but without MPA. Reactions were run under Ar to prevent any air oxidation of generated $MV^{\bullet+}$. A bias of -0.30 V vs Ag/AgCl was applied to the slide to generate driving force for electron transfer (while remaining below the direct reduction potential of $MV^{2+/+}$) from the electrode into the VB of CdSe as diagrammed in Figure 7, and the reaction was illuminated with white LEDs. Even after 1 h of irradiation, however, no $MV^{\bullet+}$ was observed spectrophotometrically.

One possible explanation for this is that reduced $MV^{\bullet+}$ is reacting with an exposed portion of the *nanoITO*, which (at -0.3 V vs. Ag/AgCl) is able to re-oxidize the $MV^{\bullet+}$ resulting in no net chemistry. To test this hypothesis, ZrO_2 was electrochemically deposited onto a CdSe sensitized electrode. ZrO_2 is a wide band-gap semiconductor that should act as an insulating material and can be easily deposited onto electrode surfaces via a reductive electrodeposition procedure from aqueous solutions of zirconyl chloride.¹⁸ A benefit to using electrodeposition is that the ZrO_2 will deposit onto the more electroactive areas of the *nanoITO*-CdSe, i.e. the exposed *nanoITO*. ZrO_2 was electrodeposited using the *nanoITO*-CdSe slide as a working electrode in a three electrode cell with a Ag/AgCl reference, and Pt wire counter by taking 20 cyclic voltammetric scans from -1.1 V to 0 V vs Ag/AgCl in an aqueous solution containing 5.0 mM $ZrOCl_2 \cdot 8H_2O$ and 0.1 M KCl. During these scans a significant decrease in current passed was observed, indicating the formation of an insulating layer of ZrO_2 (Figure S12). Using the ZrO_2 -coated *nanoITO*-CdSe slides in photoelectrochemical experiments for the reduction of MV^{2+} with light and no sacrificial electron donor as previously described, however, still did not result in any formation of $MV^{\bullet+}$ in the bulk solution.

Linear sweep voltammetry (LSV) of the *nanoITO*-CdSe photoelectrodes was performed using a chopped light source to investigate the lack of photoelectrochemical reduction of MV^{2+} . The *nanoITO*-CdSe slides both either with or without added ZrO_2 were used as the working electrode in the same three electrode set-up as for the photoelectrochemical experiments with pH = 7.4 phosphate buffer containing 5 mM

MV^{2+} . The potential was swept from 0 V to -0.8 V vs. Ag/AgCl (past the first reduction, $MV^{2+/+•}$) at a rate of 5 mV/s with chopped white light from a white LED source at 0.2 Hz. The photoresponse of the *nanol*ITO-CdSe electrode without ZrO_2 is shown in Figure 6. At more positive potentials, small amounts of current are photogenerated, but these currents are photoanodic meaning electrons are moving *into* the electrode from the CB of the excited CdSe, opposite of the desired trend. Upon reaching -0.3 V where the photoelectrochemical experiments were performed, and through the first reduction wave of MV^{2+} , little to no photoresponse is observed. Events leading to MV^{2+} reduction as depicted in Figure 7 should lead to an increase (positive currents in Figure 6) of current flow out of the electrode when the light is turned on. The results for the *nanol*ITO-CdSe electrode with the electrodeposited ZrO_2 are similar (Figure S13) with a larger magnitude photoanodic response at potentials more positive than the $MV^{2+/+•}$ couple. These experiments indicate that direct reduction of $MV^{+•}$ at an exposed *nanol*ITO surface (short circuiting) is not the sole reason for lack of $MV^{+•}$ produced in bulk solution during the photoelectrochemical experiments.

For the photoelectrochemical experiments, it is likely that an electron transfer to MV^{2+} after irradiation occurs rapidly (k_1 ,

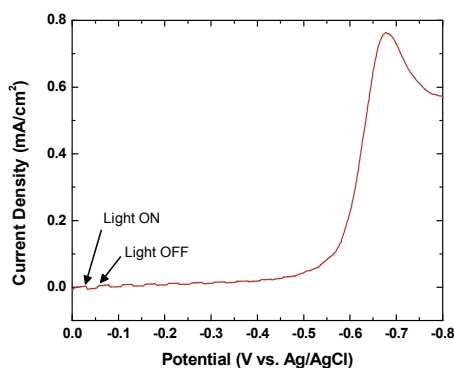


Figure 6. Linear Sweep Voltammogram of 5 mM MV^{2+} in pH = 7 phosphate buffer with a *nanol*ITO-CdSe slide as a working electrode, Pt wire counter electrode, and Ag/AgCl reference. Scan rate 5 mV/s with a chopped white light cycled on and off every 5 seconds.

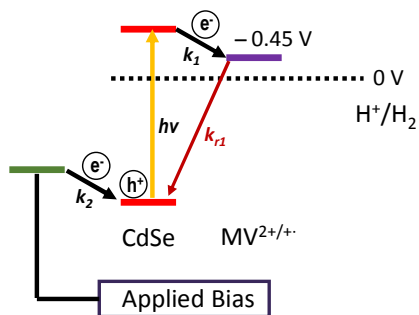
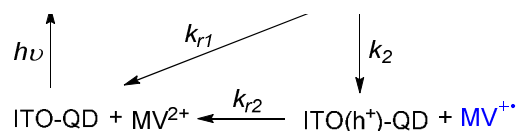


Figure 7. Cartoon of the relative energy levels of the CdSe conduction and valence bands, the oxidation potential held at the electrode, the $MV^{2+/+•}$ couple, and the proton reduction couple at pH = 0.

Scheme 1). The timescale of this reaction has been shown to be on the fs – ps timescale even in the absence of sacrificial donors,¹⁵ and the previously described quenching studies confirm this reaction will occur. However, unlike when there is a sacrificial donor in high concentration in solution, the hole left in the VB of the CdSe must be filled by an electron transferred from the *nanol*ITO surface through the organic ligands anchoring the QD to the electrode (k_2 , Scheme 1), all before back electron transfer from the $MV^{+•}$ to the hole in the VB of the CdSe can occur (k_{r1} , Scheme 1). This BET process is also likely fast and out-competes productive electron transfer from the electrode. A possible solution to this would be to switch to a conjugated ligand to link the CdSe to the *nanol*ITO surface in order to improve the electronic communication. Since terephthalic acid is competent to attach CdSe to the surface and is a conjugated linkage, LSV experiments in light and dark (Figure S14) as well as chopped light LSV experiments (Figure S15) were performed on *nanol*ITO-CdSe electrodes with terephthalic acid linkers. These results do not vary significantly from the MPA results and do not show the desired photocathodic behaviour toward the reduction of MV^{2+} . An explanation of this behaviour may be that holes are quickly trapped on surface states in the CdSe QDs and these states may be spatially separated from the surface of the *nanol*ITO electrode. If this were the case then communication between the electrode and the CdSe at one point would not have much of an effect since electrons would need to either migrate through the CdSe dots or hop around the outside of the QDs on electroactive species in solution to the hole trap.

Although photoelectrochemical experiments have proven unsuccessful, the quenching experiments demonstrate the viability of reduction reactions occurring at photocathode surfaces sensitized with QDs. In order to overcome the deleterious BET reactions preventing photoelectrochemical reduction, a thin p-type transparent semiconductor may need to be deposited on the *nanol*ITO (Figure S10) using techniques such as electrodeposition and ALD or PLD, which has already been done for n-type semiconductors like TiO_2 on *nanol*ITO.¹⁹ Other ligand exchange strategies or post-synthetic modifications of the films may also be necessary to either localize hole-traps near the *nanol*ITO interface or remove them from the CdSe QDs. One advantage of the *nanol*ITO is it provides the high surface area structure while remaining transparent, which avoids the need to make bulk wide band gap and nanostructured p-type materials. It is also advantageous to have only a thin layer of p-type semiconductor so that charges may be quickly extracted for more efficient devices.

Scheme 1. Electron Transfer Following Photoexcitation.



Experimental

Materials and Methods. Selenium dioxide, 3-mercaptopropionic acid (99+%), iodomethane (Cu stabilized ReagentPlus®, 99%), tetrabutylammonium hexafluorophosphate (for electrochemical analysis, ≥99%), ferrocene, 1-octadecene technical grade, 90%), oleic acid (technical grade, 90%), bromotrimethylsilane (>97%), and fluoride-doped tin oxide (FTO) coated glass (L×W×D 100 mm × 100 mm × 2.3 mm, surface resistivity ~7 Ω/sq, cut into 3 mm × 10 mm slides), were purchased from Sigma-Aldrich and used as received. 4,4'-bipyridine (98%), 1,2-ethylenediphosphonic acid, and 3-bromopropionic acid were purchased from Alfa Aesar. Diethyl 4-aminobenzylphosphonate was purchased from Acros Organics. Terephthalic acid was purchased from TCI America. Tin-doped indium oxide nanoparticles (*nanITO*, 99.99%, In₂O₃:SnO₂=90:10, 20-40 nm, blue powder) were purchased from Infrastructure Nanomaterials (inframat). Phosphate buffered saline solution (pH = 7.4) and ethyl acetate were purchased from Fisher Scientific. Glacial acetic acid was purchased from Macron Fine Chemicals and ethanol (200 proof) was purchased from Decon Laboratories, Inc. NMR solvents were purchased from Cambridge Isotope Labs and used as received. Cadmium myristate was synthesized from a literature procedure.¹¹ ¹H NMR spectra were collected with a 300 MHz Bruker Avance spectrometer. UV/vis spectra were collected with a Cary 5000 spectrophotometer from Agilent. SEM images were taken using a FEI Siron SEM. Electrochemical analyses were performed with a BASi Epsilon Electrochemical Workstation using a platinum auxiliary electrode (BASi) and a Ag/AgCl (3 M, BASi) reference electrode for aqueous experiments and a Ag/AgNO₃ reference (BASi) for electrochemistry in acetonitrile. White LEDs for illumination experiments consisted of a RGB LED flex strip (non-waterproof, double density, 12 V), 12 V DC Regulated Power Supply (3.5 A commercial, 40 W power supply), and IEC 3 wire power cord purchased from Creative Lighting Solutions, LLC.

Synthesis of 4-aminobenzylphosphonic acid. Diethyl 4-aminobenzylphosphonate (2.0 g, 8.2 mmol) was dissolved in anhydrous DCM (30 mL) and degassed with N₂. To the reaction was added bromotrimethylsilane (2.4 mL, 2.8 g, 18 mmol) and the reaction was stirred at room temperature for 2 d. Anhydrous methanol (2.0 mL) was then added and an off-white solid precipitated. The solid was filtered and washed with DCM and Et₂O to give 1.51 g (98 %).

Synthesis of methylviologen-iodide salt [MV](I)₂. A solution of 4,4'-bipyridine (2.0 g, 13 mmol) in CH₃CN (30 mL) was degassed with N₂. To the reaction was added MeI (4.0 mL, 9.1 g, 64 mmol) and the reaction was heated at reflux for 16 h. A deep orange solid had precipitated from the reaction. The reaction was allowed to cool to room temperature and the solid was filtered and washed with CH₃CN (30 mL) and Et₂O (30 mL) to give 5.5 g (96 %) of product.

¹H NMR (300 MHz, CD₃OD): δ 8.96 (d, 4H), 8.43 (d, 4H), 4.41 (s, 6H)

Synthesis of N-methyl-4,4'-bipyridine (monoquat)-iodide salt [MQ](I). A solution of 4,4'-bipyridine (3.0 g, 19 mmol) in

EtOAc (30 mL) was degassed with N₂. To the reaction was added MeI (2.4 mL, 5.6 g, 38 mmol) and the reaction was heated at reflux for 3 h. A bright yellow solid had precipitated from the reaction. The reaction was allowed to cool to room temperature and the solid was filtered and washed with EtOAc (30 mL) and Et₂O (30 mL) to give 4.8 g (85 %) of product.

¹H NMR (300 MHz, CD₃OD): δ 9.07 (d, 2H), 8.85 (d, 2H), 8.54 (d, 2H), 8.02 (d, 2H), 4.50 (s, 3H)

Synthesis of N-methyl-N'-propionic acid-viologen-mixed salt [MV-COOH](Br)(I). A solution of 2.0 g (6.7 mmol) [MQ](I) and 2.1 g (13 mmol) Br(CH₂)₂COOH in CH₃CN (30 mL) were degassed with N₂. The reaction was heated at reflux for 16 h. An orange solid had precipitated and it was filtered and washed with CH₃CN (30 mL) and Et₂O (50 mL) to give 2.74 g (91 %) of an orange powder.

¹H NMR (300 MHz, CD₃OD): δ 9.09 (d, 2H), 8.95 (d, 2H), 8.42 (t, 4H), 4.89 (t, 2H) 4.40 (s, 3H), 3.11 (t, 2H)

General procedure for photochemical reduction experiments in solution. CdSe QDs were obtained as a solution in pentane. An amount of stock solution containing 1.63 × 10⁻⁸ mol CdSe was added to a vial and the solvent was removed. A solution containing 5 mM [MV](I)₂ and 50 mM MPA in pH = 7.4 PBS buffer (2.5 mL) was added to an amount of CdSe QDs and the mixture was sonicated for 20 minutes to suspend the QDs. The solution was added to a cuvette along with a miniature stir-bar and closed with a septum-cap. The reaction was degassed for 10 min by flowing N₂ through the solution. This cuvette was kept under N₂ and placed in the middle of a crystallizing dish filled with water that was wrapped with white LED lights (Figure S6). The lights were held approximately 10 cm from the reaction at which distance the measured power was 2.0 mW/cm². Spectral output of the white LEDs is shown in Figure S1. The solution was illuminated for 20 minutes and at various time points was removed and a UV/vis spectrum was collected. The amount of MV^{•+} present was calculated based on the extinction coefficient at 603 nm.

General procedure for photochemical reduction experiments of nanoITO slides. A solution containing 5 mM [MV](I)₂ and 50 mM MPA in pH = 7.4 PBS buffer (5 mL) along with a stir bar was added to a clear glass vial with a gas-tight screw cap with a septum. A slide of *nanITO* loaded with CdSe via MPA linker (dipping cycles as described in the paper) was then added and the vial was sealed. The solution was bubble degassed with N₂ for 10 min and kept under N₂. The reaction was then illuminated with LED lights in the same set-up (Figure S6) for 20 min. Aliquots were taken at various time points and injected into a cuvette that was kept under N₂ through a septum cap. UV/vis spectra were recorded to obtain the amount of MV^{•+} produced.

Conclusions

We have demonstrated the ability to use CdSe QDs to functionalize high surface area, transparent electrodes for photo-driven reduction reactions. The electrodes were made out of *nanITO* which is a transparent conducting oxide that can easily be applied to glass substrates to create high surface

area scaffolds which are necessary for photoelectrochemical water splitting device designs. Sensitized electrodes were used to photochemically reduce MV^{2+} which demonstrated the ability to drive reactions at the surface of the electrodes using light. Although the current version of the sensitized electrodes were not able to photoelectrochemically reduce MV^{2+} , these materials represent an important step toward second generation devices where electrode morphology does not need to be controlled by a semiconducting material that also must act as light absorber, thus removing some of the challenging limitations in finding new p-type materials and dyes for photocathode applications.

Notes and references

1. E. S. Andreiadis, M. Chavarot-Kerlidou, M. Fontecave and V. Artero, *Photochem. Photobiol.*, 2011, **87**, 946.
2. J. H. Alstrum-Acevedo, M. K. Brennaman and T. J. Meyer, *Inorg. Chem.*, 2005, **44**, 6802; D. Gust, T. A. Moore and A. L. Moore, *Acc. Chem. Res.*, 2009, **42**, 1890; M. G. Walter, E. L. Warren, J. R. McKone, S. W. Boettcher, Q. Mi, E. A. Santori and N. S. Lewis, *Chem. Rev.*, 2010, **110**, 6446.
3. P. V. Kamat, *J. Phys. Chem. C*, 2008, **112**, 18737; M. Shalom, I. Hod, Z. Tachan, S. Buhbut, S. Tirosh and A. Zaban, *Energy Environ. Sci.*, 2011, **4**, 1874.
4. P. V. Kamat, *J. Phys. Chem. Lett.*, 2013, **4**, 908.
5. V. González-Pedro, I. Zarazua, E. M. Barea, F. Fabregat-Santiago, E. de la Rosa, I. Mora-Seró and S. Giménez, *J. Phys. Chem. C*, 2013, **118**, 891; O. Khaselev and J. A. Turner, *Science*, 1998, **280**, 425.
6. H. Zhu, N. Song, H. Lv, C. L. Hill and T. Lian, *J. Am. Chem. Soc.*, 2012, **134**, 11701; L. Amirav and A. P. Alivisatos, *J. Phys. Chem. Lett.*, 2010, **1**, 1051.
7. Z. Han, F. Qiu, R. Eisenberg, P. L. Holland and T. D. Krauss, *Science*, 2012, **338**, 1321.
8. I. Barceló, E. Guillén, T. Lana-Villarreal and R. Gómez, *J. Phys. Chem. C*, 2013, **117**, 22509.
9. L. Gao, Y. Cui, J. Wang, A. Cavalli, A. Standing, T. T. T. Vu, M. A. Verheijen, J. E. M. Haverkort, E. P. A. M. Bakkers and P. H. L. Notten, *Nano Lett.*, 2014, **14**, 3715.
10. G. Hoertz Paul, Z. Chen, A. Kent Caleb and J. Meyer Thomas, *Inorg. Chem.*, 2010, **49**, 8179.
11. O. Chen, X. Chen, Y. Yang, J. Lynch, H. Wu, J. Zhuang and Y. C. Cao, *Angew. Chem., Int. Ed.*, 2008, **47**, 8638.
12. W. W. Yu, L. Qu, W. Guo and X. Peng, *Chem. Mater.*, 2003, **15**, 2854.
13. B. H. Farnum, Z. A. Morseth, A. M. Lapidés, A. J. Rieth, P. G. Hoertz, M. K. Brennaman, J. M. Papanikolas and T. J. Meyer, *J. Am. Chem. Soc.*, 2014, **136**, 2208.
14. M. M. Collinson, *ISRN Analytical Chemistry*, 2013, **2013**, 21.
15. A. J. Morris-Cohen, M. D. Peterson, M. T. Frederick, J. M. Kamm and E. A. Weiss, *J. Phys. Chem. Lett.*, 2012, **3**, 2840.
16. K. E. Knowles, E. A. McArthur and E. A. Weiss, *ACS Nano*, 2011, **5**, 2026.
17. T. Watanabe and K. Honda, *J. Phys. Chem.*, 1982, **86**, 2617.
18. H.-Z. Yu, A. W. Rowe and D. M. Waugh, *Analytical Chemistry*, 2002, **74**, 5742.
19. L. Alibabaei, B. H. Farnum, B. Kalanyan, M. K. Brennaman, M. D. Losego, G. N. Parsons and T. J. Meyer, *Nano Lett.*, 2014, **14**, 3255.